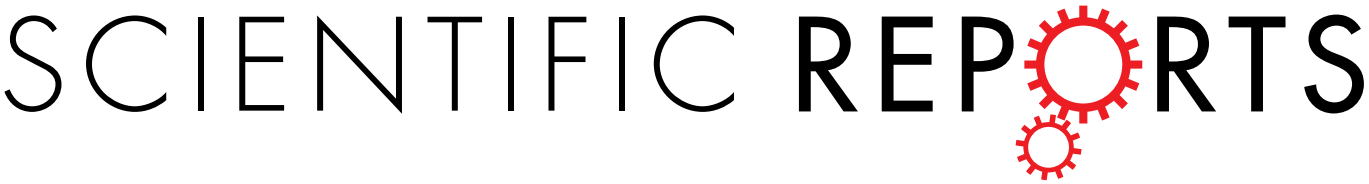

OPEN

Amplifying the signal of localized surface plasmon resonance sensing for the sensitive detection of Escherichia coli O157:H7

Received: 9 January 2017
Accepted: 28 April 2017
Published online: 12 June 2017

Liping Song[1,2], Lei Zhang[2], Youju Huang[2], Liming Chen[2], Ganggang Zhang[2], Zheyu Shen[2], Jiawei Zhang[2], Zhidong Xiao[1] & Tao Chen[2]

Gold nanorods (Au NRs) based localized surface plasmon resonance (LSPR) sensors have been widely employed in various fields including biology, environment and food safety detection, but their size- and shape-dependent sensitivity limits their practical applications in sensing and biological detection. In our present work, we proposed an approach to maximally amplify the signal of Au NRs based LSPR sensing by coating an optimized thickness of mesoporous silica onto Au NRs. The plasmonic peaks of Au NRs@SiO_2 with different shell thickness showed finely linear response to the change of surrounding refractive index. The optimized thickness of mesoporous silica of Au NRs@SiO_2 not only provided high stability for LSPR sensor, but also displayed much higher sensitivity (390 nm/RIU) than values of Au NRs from previous reports. The obtained Au NRs@SiO_2 based LSPR sensor was further used in practical application for selectively detection of the *E. coli* O157:H7, and the detection limit achieved 10 CFU, which is much lower than conventional methods such as electrochemical methods and lateral-flow immunochromatography.

The localized surface plasmon resonance (LSPR) is a spectroscopic phenomenon based on the resonant oscillations of free electrons of various materials including noble metal nanoparticles, Al nanoparticles, conventional semiconductors and 2D materials, when stimulated by incident light[1–3]. Except the size, shape[4,5] and composition of nanoparticles, the frequency and intensity of the LSPR bands are sensitive to the interparticle spacingno and dielectric environment[6,7]. Therefore, the response of plasmonic nanoparticles to the refractive index variation of surrounding medium is employed to develop LSPR sensors in broad fields of biology, food, and environment[8–11]. However, due to the low detection sensitivity and capacity[7,12,13] and poor stability, the development of LSPR sensors is limited, especially in practical applications. For example, numerous efforts have been devoted to develop various methods for the detection of *E. coli* O157:H7, which is a gram-negative enteric bacteria, causing severe intestinal infections in humans[14,15]. Traditional methods [16–18] such as electrochemical methods and lateral-flow immunochromatography for detecting *E. coli* O157:H7 are always time-consuming and the sensitivity is not very high[19–21] and limits their practical use as a commercial product. The objective of the present study is to develop a high performance LSPR sensor for practical application in real sample analysis (*E. coli* O157:H7) that would achieve high sensitivity and stability.

In recent years, some strategies were suggested to improve the sensitivity and stability of LSPR sensors such as morphology optimization of nanoparticles, surface functionalization and single nanoparticle detection[22,23]. Meanwhile, surface functionalization served as a powerful means not only to effectively improve sensitivity and stability of LSPR sensors but also flexibly modify plasmonic nanoparticles with desired functions for further applications[24]. For example, polymer or biomolecules coated Au nanoparticles LSPR sensors show higher selectivity and stability[25].

[1]Department of Chemistry, Huazhong Agricultural University, Wuhan, 430070, China. [2]Key Laboratory of Marine Materials and Related Technologies, Zhejiang Key Laboratory of Marine Materials and Protective Technologies, Ningbo Institute of Materials Technology and Engineering, No. 1219 Zhongguan West Road, Ningbo, 315201, China. Correspondence and requests for materials should be addressed to Y.H. (email: yjhuang@nimte.ac.cn) or Z.X. (email: zdxiao@mail.hzau.edu.cn) or T.C. (email: tao.chen@nimte.ac.cn)

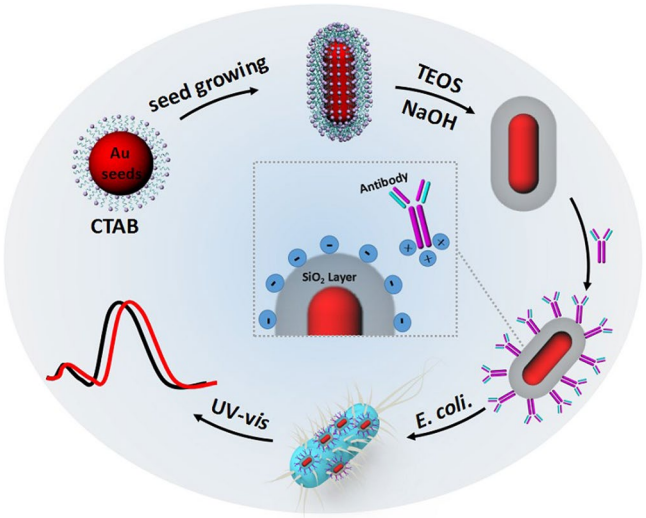

Figure 1. Schematic illustration of the synthesis of Au NRs and Au NRs@SiO_2 and the procedure of detection for *E. coli* O157:H7.

Homogeneous mesoporous silica has been proven to be a versatile biomaterial to directly improve stability of nanoparticles in complex bio-system, due to its excellent biocompatibility. On the other hand, mesoporous structure[26–28] provides large-area and easy-decorated surface for maximally capturing the target molecules to improve the sensitivity of LSPR. Since the encapsulated SiO_2 determines the refractive index of surrounding environment, the thickness of SiO_2 attributed to a vital parameter to affect LSPR sensitivity. However, there is a controversial point about the effect of thickness of SiO_2 shell on LSPR sensitivity. For instance, Xu and co-workers synthesize 8 nm mesoporous silica shell coated Au NRs to improve the sensitivity to 325 nm/RIU[22]. Wang and co-workers used 21 nm silica coated Au NRs to amplify the sensitivity for detecting biomolecules[29]. Moreover, Huang and co-workers considered that a 2–3 nm silica shell coated on Au NRs induces a highest sensitivity for plasmonic organic photovoltaic devices[30]. The recent theoretical calculation reveals that ultrathin silica coating (within 3.5 nm) would be ideal for improving the sensitivity[31]. Therefore, the aim of our present work is to explore the cut-off thickness in a small size, and further amplify the sensitivity of Au NRs maximally for practical application for detection of *E. coli* O157:H7.

Herein, a series of Au nanorods (Au NRs) with different mesoporous silica shell are synthesized to study the effects of silica shell thickness on the sensitivity of Au NRs LSPR symmetrically. The as-prepared Au NRs@SiO_2 with optimal shell thickness showed high sensitivity and used as efficient LSPR biosensor to detect *E. coli* O157:H7. Au NRs with elongated geometry were selected as plamonic nanoparticles for LSPR sensor due to their tunable and broad spectra range from the visible to near-infrared region[24,32,33]. The thickness of SiO_2 on AuNRs was optimized by adjusting the concentration of Cetyltrimethyl Ammonium Bromide (CTAB) and the amount of tetraethyl orthosilicate (TEOS), achieving sensitive Au NRs@SiO_2. To verify the performance of Au NRs@SiO_2 as LSPR sensors, Au NRs@SiO_2 with optimal thickness was modified with specific antibody to selectively detect *E. coli* O157:H7 in high sensitivity. The detection limit of Au NRs@SiO_2 for *E. coli* O157:H7 is lower than 10 Colony-Forming Units (CFU), which is superior over the values of traditional methods[34,35].

Results and Discussion

Au NRs (Fig. 1 and 2A) were synthesized by using the seed-mediated growth method[36], which has an aspect ratio of 2.9. As prepared Au NRs showed typical horizontal and longitudinal LSPR bands at 530 nm and 726 nm, respectively (Fig. 2C). The number of Au NRs in solution was estimated to be 2.1 nM according to its extinction coefficient ($3.9 \pm 0.5 \times 10^9\,M^{-1}\,cm^{-1}$) at the longitudinal plasmon peak (726 nm)[37,38]. According to the traditional method (soft-templating method), Au NRs were uniformly coated with mesoporous silica, forming monodispersed core-shell AuNRs@SiO_2 nanostructures (Fig. 1 and 2B)[39]. In the process of silica coating, CTAB formed a bilayer around Au NRs, which served as organic template for the formation of mesoporous silica shell[40]. Moreover, it was found that the longitudinal LSPR band of Au NRs@SiO_2 redshifted clearly compared with Au NRs (Fig. 2C), leading to a lighter pink color (illustration of Fig. 2D).

In order to study systematically the influence of silica thickness on the LSPR of Au NRs@SiO_2, Au NRs@SiO_2 with different shell thickness were prepared by adjusting the concentration of CTAB and the amount of TEOS. When the additive amount of TEOS was changed from 2 μL to 20 μL, the silica shell thickness increased from 2 nm to 25 nm (Fig. 3). It is noteworthy that the thickness of silica was calculated according to the general theory of statistics by measuring more than 100 particles. Fig. S1 showed the statistical values and statistical distribution of Au NRs@SiO_2 with 2 nm SiO_2 layer. The thickness of other SiO_2 layers on Au NRs@SiO_2 (5, 10, 15, 20, 25 nm) were also confirmed by the general theory of statistics. CTAB was used as the template for depositing silica and many previous reports showed that lower concentration of CTAB resulting in thicker silica shell[41–43]. Therefore, by adjusting the concentration of CTAB and the amount of TEOS, Au NRs@SiO_2 with different shell thickness could be prepared. The uniform silica shell endows a protective layer on the surface of Au NRs, leading

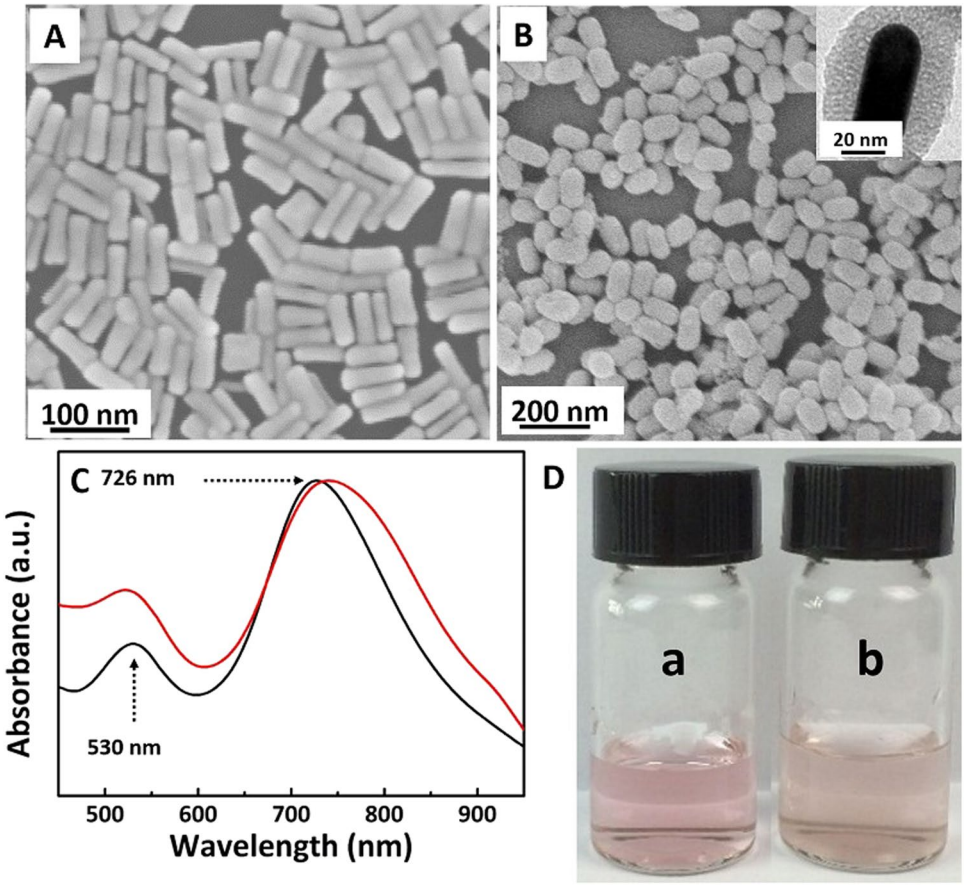

Figure 2. SEM (**A**) and TEM (**B**) of as-prepared Au NRs and Au NRs@SiO_2, respectively; (**C**) UV-vis spectra of Au NRs (black) and Au@SiO_2 (red); (**D**) Photographs of Au NRs (a) and Au@SiO_2 (b).

to extremely stable Au NRs dispersion that could keep for three months at room temperature even after removal of CTAB.

Furthermore, the LSPR properties of Au NRs with different mesoporous silica shell were investigated by UV-*vis* absorption spectra (Fig. 4). The longitudinal plasmon bands of Au NRs@SiO_2 redshifted gradually with increasing the thickness of silica shell (Fig. 4A). The relationship between plasmon shift and thickness of silica is shown in Fig. 4B, indicating that the plasmon band shift showed approximately linearly with increasing shell thickness. This was ascribed to the refractive index variation of silica shell when changing the thickness[27]. The refractive index of porous silica is much higher than the value of water. When the porous silica was coated onto the surfaces of Au NRs, the refractive index of surrounding environment of Au NRs increased, which was in accordance with previous work[44]. Therefore, the coating of silica on Au NRs led to redshift of the longitudinal plasmon band, which proved that the Au NRs@SiO_2 was much sensitive to the change of surrounding refractive index than Au NRs. This allowed Au NRs@SiO_2 could be employed as a LSPR sensor based on the redshift of longitudinal plasmon band induced by coating with mesoporous silica.

To verify the performance of the Au NRs@SiO_2 based LSPR biosensor, Au NRs@SiO_2 was firstly used to test the surrounding refractive index variations, as shown in Fig. 5. The sensitivity was calculation according to the universal experienced formula[45]:

$$\triangle\lambda = m \cdot \triangle n \quad (1)$$

$\Delta\lambda$ is the difference of the LSPR wavelength before and after coating; m is the sensitivity, Δn is the change in the refractive index.

The refractive index was tuned by adjusting the volume ratio of water and glycerol (from 0.9 to 0.1 with the volume ratio of 0.1 interval), and the refractive indices of the mixture solvents were calculated based on the Lorentz-Lorenz equation, as shown in the experimental details[23,46]. Both of Au NRs and Au NRs@SiO_2 exhibited band redshift when increasing the volume ratio of glycerol to water (Fig. 5A and B).

The plasmon peaks of Au NRs and Au NRs@SiO_2 in mixed solution was plotted against with refractive index, as shown in Fig. 5C. It was found that plasmon absorption shifts linearly to longer wavelength with increasing the refractive index[22,47,48]. In addition, only absorption is considered here and the influence of scattering are neglected due to higher absorption than scattering of nanorods[49].

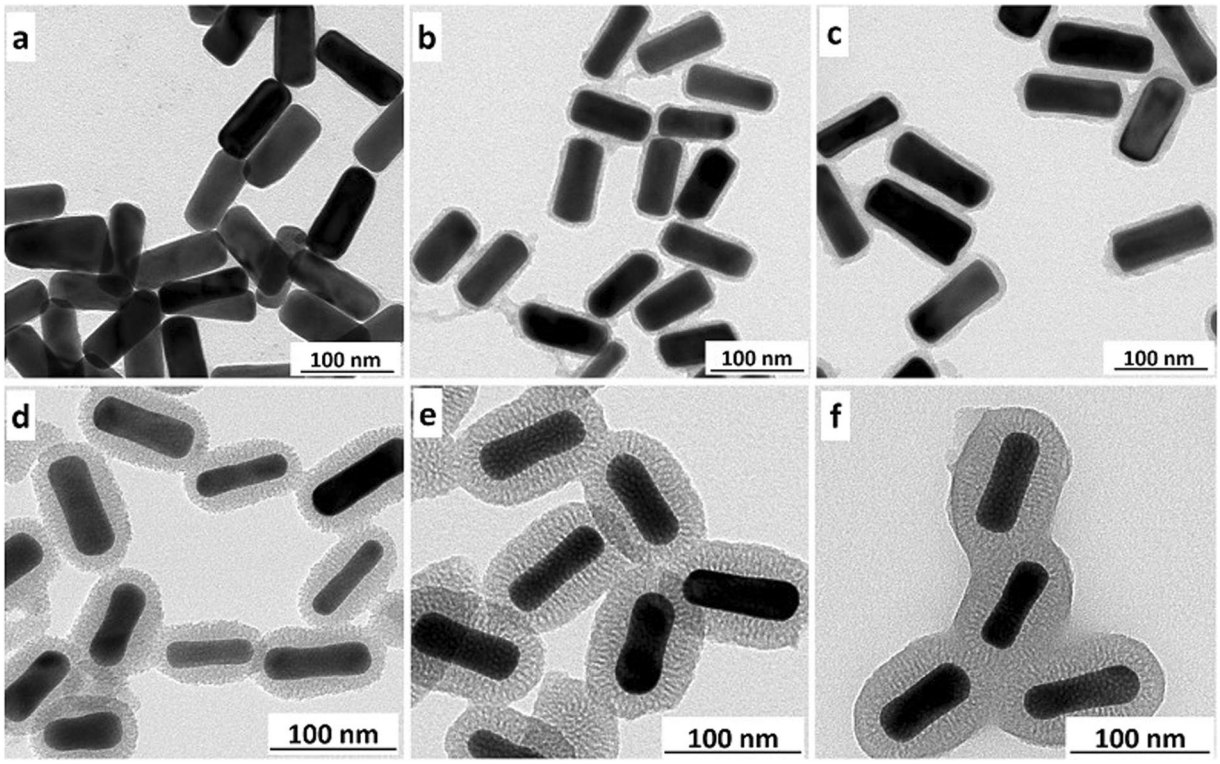

Figure 3. TEM images of Au NRs@SiO_2 with different shell thickness. The thickness of silica were as follows, respectively: (**a**) 2 nm; (**b**) 5 nm; (**c**) 10 nm; (**d**) 15 nm; (**e**) 20 nm; (**f**) 25 nm.

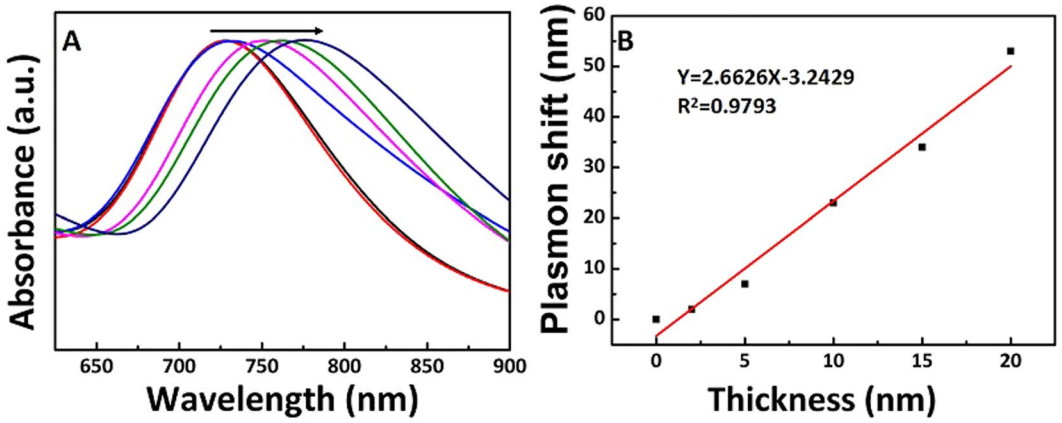

Figure 4. (**A**) Normalized extinction spectra of Au NRs@SiO_2 with different shell thickness from 2 nm to 20 nm; (**B**) Linearity curve of plasmon shift vs. the thickness of silica.

The slope indicated the refractive index sensitivities, as shown in Fig. 5D. The sensitivity values of Au NRs@SiO_2 with different thickness were ranged from 110 nm/RIU to 390 nm/RIU. The Au NRs@SiO_2 with 2 nm shell exhibited highest sensitivity approaching to 390 nm/RIU, which was much higher than that of previous reports (the reported highest value was 325 nm/RIU)[22,33,50]. The sensitivity of Au NRs@SiO_2 had intimate relation with the silica shell and reduced gradually with increasing the shell thickness, which agreed with the results in previous work[22,31]. The sensitivity of Au NRs@SiO_2 with 2 nm or 5 nm shell was larger than the values of Au NRs and the Au NRs@SiO_2 with other thickness. Generally, the improvement in sensitivity can be explained according to the universal experienced formula[50–53]

$$\Delta\lambda = m(n_{adsorbate} - n_{medium})(1 - e^{-\frac{2d}{l_d}}) \quad (2)$$

$\Delta\lambda$ is the difference of the LSPR wavelength before and after coating; m is the sensitivity; $n_{adsorbate}$ and n_{medium} are the refractive indexes of the shell and the solution, respectively; d is the thickness of the coating shell and l_d is the electromagnetic field decay length of the system, make A equal to $(1 - e^{-\frac{2d}{l_d}})$.

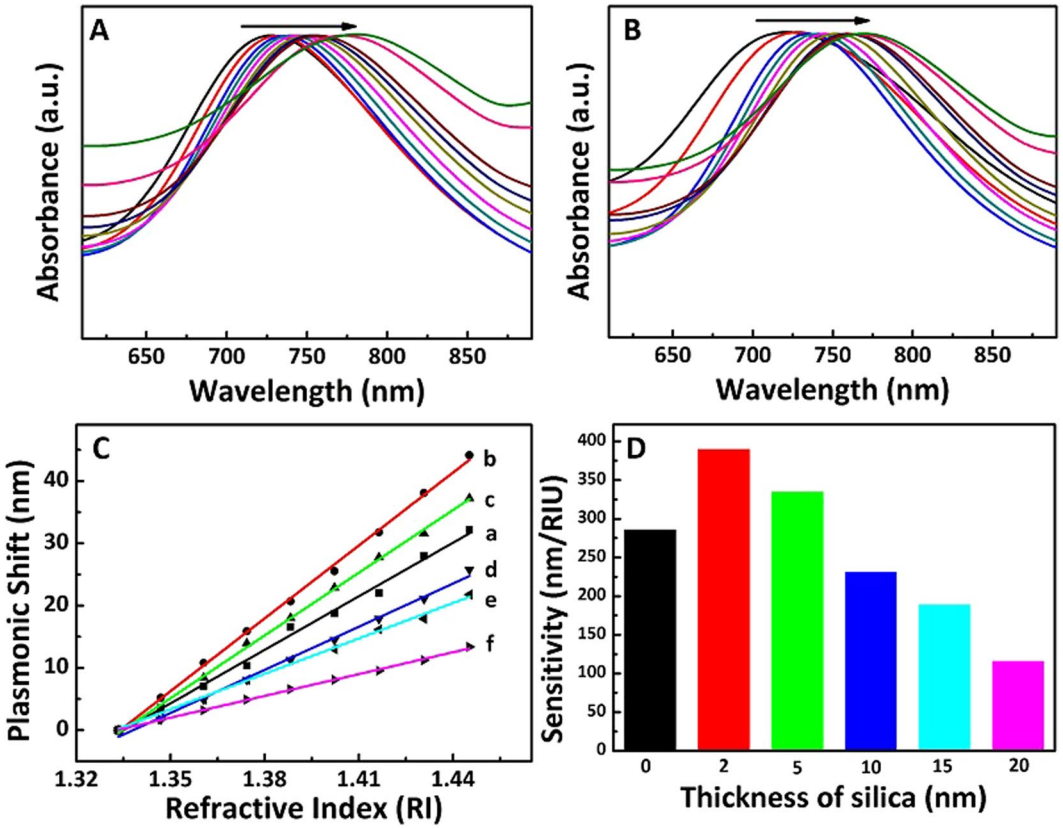

Figure 5. Normalized extinction spectra of Au NRs (**A**) and Au NRs@SiO_2 with 2 nm shell thickness (**B**) in a mixture of water and glycerol with different volume ratios from 0.9 to 0.1 with the volume ratio of 0.1 interval; (**C**) Comparison of the refractive index sensitivity of Au NRs (a) and Au NRs@SiO_2 with different SiO_2 thickness from 2 nm to 20 nm (cross ponding to b to f); (**D**) Difference in sensitivity of Au NRs and Au NRs@SiO_2 with different SiO_2 thickness from 2 nm to 20 nm.

When Au NRs coated with thin silica, the change of A was ignored due to the minor change of d. The sensitivity was determined by the value of $\Delta\lambda/\Delta n$, which resulted in higher sensitivity than Au NRs due to higher change of $\Delta\lambda$ than Δn. However, when the silica shell became much thicker, the change of *d* can't be ignored, which resulted in the increase of A. Though the value of $\Delta\lambda$ increased, the sensitivity decreased following the increase of Δn and A. Therefore, it is not uncommon that the Au NRs@SiO_2 with 2 nm shell was with the highest sensitivity for about 390 nm/RIU.

Au NRs@SiO_2 with 2 nm of shell thickness showed optimal sensitivity of 390 nm/RIU and can serve as ideal candidate for high-efficiency LSPR sensors. Au NRs@SiO_2 was modified with specific antibody to selectively detect *E. coli* O157:H7. Due to the negative shell, the surface of the Au NRs@SiO_2 was negatively charged, which provided opportunity for the electrostatic interaction between Au NRs@SiO_2 and the positive antibody (Fig. S2) and simplified the procedure and avoided extra chemical treatment. *E. coli* O157:H7 samples with different concentration were mixed with antibody-conjugated Au NRs@SiO_2 to promote the sufficient incubation. Then the typical plasmon band shifts of Au NRs were measured using UV-*vis* absorption spectra to detect *E. coli* O157:H7 (Fig. 6A). After integrated with *E. coli* O157:H7, the longitudinal plasmon band of Au NRs@SiO_2 redshifted gradually and the absorption intensity was decreased gradually when increasing the concentration of *E. coli* O157:H7 in the range from 0 to 0.5×10^5 CFU (Fig. 6A).

Au NRs@SiO_2 was sensitive to the surrounding refractive. With increasing the concentration of *E. coli* O157:H7, the refractive index around Au NRs@SiO_2 increased, which led to the redshift of the longitudinal plasmon band[24]. The relationship between plasmon band shift and logarithmic concentration of *E. coli* O157:H7 is shown in Fig. 6B. It was found that the redshift changed linearly with the logarithmic concentration of *E. coli* O157:H7, which made it possible to detect *E. coli* O157:H7 quantitatively. Furthermore, the experiment of the selectivity of the sensor had been done by using Salmonella Typhimurium (S. Typhimurium) with the antibody of *E. coli* O157:H7 (Fig. S3) to replace *E. coli* O157:H7. The LSPR band of Au NRs@SiO_2 was almost unchanged except some negligible change (around 0.5 nm). The results indicated that the antibody-conjugated Au NRs@SiO_2 only bind to *E. coli* O157:H7 due to the specific recognition.

Conclusion

In summary, a highly sensitive plasmon resonance biosensor based on Au NRs@SiO_2 was prepared to detect *E. coli* O157:H7 quickly and simply. By adjusting the concentration of CTAB and the amounts of TEOS, we

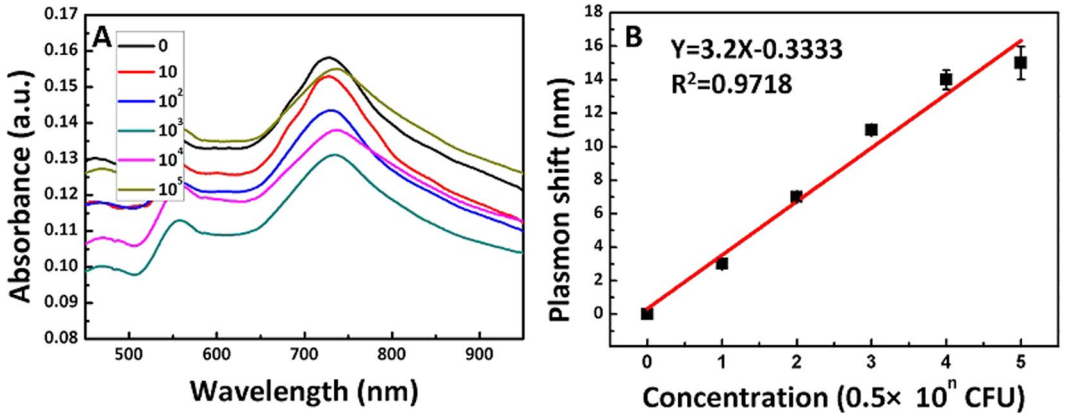

Figure 6. (**A**) UV-vis spectra of Au NRs@SiO_2 after reaction with different concentrations (from 0 to 0.5×10^6 CFU) of *E. coli* O157:H7 in the 0.01 M PBS solutions (pH = 7.4); (**B**) Linearity curve for the plot of plasmon shift vs. the logarithm of concentration of *E. coli* O157:H7 (n = 1, 2, 3, 4, 5, 6).

synthesized monodisperse Au NRs@SiO_2 with serious uniform silica shell. Meanwhile, the refractive index sensitivities of both Au NRs and Au NRs@SiO_2 with different thickness of silica shell were investigated and the Au NRs@SiO_2 with 2 nm shell was most sensitive compared to others. In addition, the Au NRs@SiO_2 with 2 nm shell was used here to detect the *E. coli* O157:H7 by simply physical adsorption between antibodies and Au NRs@SiO_2. The results indicated that the plasmon shift was very sensitive to the change of the concentration of *E. coli* O157:H7 and monitoring *E. coli* O157:H7 at concentration lower than 10 CFU in less than 40 min, which meant the LSPR platform based on Au NRs@SiO_2 was sensitive, simple, quick for monitoring *E. coli* O157:H7 without any expensive instruments and this label-free method was promising to applied in detecting pathogenic agents.

Methods

Reagents and materials. Hexadecyltrimethylammonium bromide (CTAB), Sodium borohydride ($NaBH_4$) and Tetraethylorthosilicate (TEOS) were commercially available from Sigma-Aldrich Chemical Co. (St. Louis, MO, USA). L-Ascorbic Acid (AA) was purchased from Energy Chemical in Shanghai. Chloroauricacid ($HAuCl_4 \bullet 3H_2O$, 99.9%), Silver nitrate ($AgNO_3$), ethanol, hydrochloric acid (HCl) and sodium hydroxide were purchased from Sinopharm Chemical Reagent Co. Ltd. (Shanghai). *E. coli* O157:H7 (1.7×10^8 CFU/mL), Salmonella Typhimurium (S. Typhimurium) (2.48×10^8 CFU/mL) and the murine anti- *E. coli* O157:H7 monoclonal antibody were purchased from Meridian Life Science, Inc. (Memphis, TN). Phosphate buffer saline (PBS, pH = 7.4) was purchased from Sigma Chemical Company (St. Louis, MO) and was used to dilute the *E. coli* O157:H7 stock solution (1.7×10^8 CFU/mL) with different concentrations (from 10 to 10^5 CFU/mL). Other chemicals were purchased from Sinopharm Chemical Reagent Co., Ltd. (China) and used without any further purification.

Transmission electron microscopy (TEM) was performed on a JEOL JEM-2100F instrument and operated at 200 kV. Scanning electronic microscopy (SEM) measurements were carried out by a JEOL JMS-6700F scanning microscope. UV-*vis* absorption spectra were collected by virtue of TU-1810 UV-*vis* spectrophotometer provided by Purkinje General. The surface zeta potential data was performed on a Zeta Potential Analyzer.

The Synthesis of Gold Nanorods. CTAB stabilized gold nanorods were synthesized using the seed-mediated growth method with minor modifications[36,54]. First, 0.6 mL of freshly prepared ice-cold aqueous $NaBH_4$ solution (0.01 M), was added into mixed aqueous solution containing 0.25 mL, 0.01 M $HAuCl_4$ and 9.75 mL, 0.1 M CTAB. After string violently for 2 min, the seeds formed and were used within 10~120 min. The growth solution was prepared by mixing the aqueous solution of 4 mL, 0.01 M $HAuCl_4$, 0.8 mL, 0.01 M $AgNO_3$, 80 mL and 0.1 M CTAB firstly. Then 0.64 mL, 0.1 M freshly prepared aqueous ascorbic acid solution was added into the above mixture solution with gentle string, followed by adding 1.6 mL, 0.1 M HCl aqueous solution. After mixing the resultant solution with gentle string, 0.02 mL seed solution was added then mixing it with gentle inversion for 10 s and then left the growth solution undisturbed at least 6 h.

The synthesis of Au NRs@SiO_2 with different thicknesses. The synthesis of Au NRs@SiO_2 with homogeneous silica thickness was carried out according to the traditional soft-templating method[55]. The 10 mL of as-prepared Au NRs was washed using deionized water by centrifugation (6500 rpm, 10 min) for 2 times. The supernatant was removed and the pellet was diluted to 10 mL by adding deionized water. Then a certain amount of NaOH (0.1 M) was added to the above solution to adjust the solution PH to 10.6. After the solution was mixed for 20 min, three 2 μL, 4 μL, 6 μL, 10 μL, 15 μL, 20 μL injections of 20% TEOS in ethanol solution was added under gentle stirring at 30 min intervals and the solution was mixed under room temperature for 24 h.

Refractive Index Sensitivity Measurements. Water/glycerol solutions with a percentage of glycerol ranging from 0 to 90% at 10% intervals were used to change the refractive index experienced by the Au NRs and Au NRs@SiO_2. The refractive indexes were calculated according to the Lorentz-Lorenz equation as follows:

$$\frac{n_{12}^2 - 1}{n_{12}^2 + 2} = \varphi_1 \frac{n_1^2 - 1}{n_1^2 + 2} + \varphi_2 \frac{n_2^2 - 1}{n_2^2 + 2} \quad (3)$$

Wherein n_{12} is the refractive index of the mixture, n_1 (1.3334) and n_2 (1.4746) are the refractive indices of water and glycerol, respectively, φ_1 and φ_2 are their volume fractions. For sensitivity measurements, 3 mL particle samples in solvent with different concentration of glycerol were used. The location of the absorption peak changed response to the concentration variety of glycerol. The LSPR shift showed linearly dependence on the refractive index change and the slope represented the sensitivity of the corresponding sample.

Immobilization of antibodies on Au NRs@SiO_2 and Detection of *E. coli* O157:H7. Firstly, 5 mL of as-prepared Au NRs@SiO_2 was washed for 2 times by centrifugation (6500 rpm, 6 min) and redispersed into 5 mL PBS solution (pH 7.4, 0.01 M). Then 1 mL 0.1 $\mu g\,mL^{-1}$ antibodies for *E. coli* O157:H7 was added into the above solution and stirred for 30 min at room temperature. Then the antibodies conjugated Au NRs@SiO_2 was centrifuged for once to remove free antibodies and redispered into 5 mL of PBS (pH 7.4, 0.01 M). 0.5 mL *E. coli* O157:H7 with different concentrations were mixed with 0.5 mL the as-synthesized antibodies conjugated Au NRs@SiO_2. After gentle shaking for 10 min, the mixture was settled for 70 min without disturbance at 37 °C. Then the resultant solution was detected under UV-*vis* measurement. The selective experiment was similar to the above detecting experiment just replaced the *E. coli* O157:H7 with S. Typhimurium of equal volume.

References

1. Eliza, H. & Fendler, J. H. Exploitation of Localized Surface Plasmon Resonance. *Adv. Mater.* **16**, 1865–1706 (2004).
2. Knight, M. W., King, N. S., Liu, L., Everitt, H. O., Nordlander, P. & Halas, N. J. Aluminum for Plasmonics. *ACS Nano* **8**, 834–840 (2014).
3. Naik, G. V., Shalaev, V. M. & Boltasseva, A. Alternative Plasmonic Materials: Beyond Gold and Silver. *Adv. Mater.* **25**, 3264–3294 (2013).
4. Chung, T., Lee, S. Y., Song, E. Y., Chun, H. & Lee, B. Plasmonic nanostructures for nano-scale bio-sensing. *Sensors* **11**, 10907–10929 (2011).
5. Huang, Y. J. *et al*. Engineering Gold Nanoparticles in Compass Shape with Broadly Tunable Plasmon Resonances and High-Performance SERS. *ACS Appl. Mater. Interfaces* **8**, 27949–27955 (2016).
6. Elin, M., Larsson, J. A., Mikael Ka1ll and Duncan S. Sutherland. Sensing Characteristics of NIR Localized Surface Plasmon Resonances in Gold Nanorings for Application as Ultrasensitive Biosensors. *Nano Lett*. **7**, 1256-1263 (2007).
7. Anker, J. N. *et al*. Biosensing with plasmonic nanosensors. *Nat. Mater.* **7**, 442–453 (2008).
8. Chen, H. J. *et al*. Shape-Dependent Refractive Index Sensitivities of Gold Nanocrystals with the Same Plasmon Resonance Wavelength. *J. Phys. Chem. C* **113**, 17691–17697 (2009).
9. Liu, L., Ouyang, S. & Ye, J. Gold-nanorod-photosensitized titanium dioxide with wide-range visible-light harvesting based on localized surface plasmon resonance. *Angew. Chem. Int. Ed.* **52**, 6689–6693 (2013).
10. Zhou, N., Ye, C., Polavarapu, L. & Xu, Q. H. Controlled preparation of Au/Ag/SnO_2 core-shell nanoparticles using a photochemical method and applications in LSPR based sensing. *Nanoscale* **7**, 9025–9032 (2015).
11. Huang, H. W. *et al*. Preparation of controllable core-shell gold nanoparticles and its application in detection of silver ions. *ACS Appl. Mater. Interfaces* **3**, 183–190 (2011).
12. Sepúlveda, B., Angelomé, P. C., Lechuga, L. M. & Liz-Marzán, L. M. LSPR-based nanobiosensors. *Nano Today* **4**, 244–251 (2009).
13. Jing Zhao, X. Z., Yonzon, C. R., Haes, A. & Duyne, Richard,P. Van Localized surface plasmon resonance biosensors. *Nanomedicine* **1**, 219–228 (2006).
14. Li, Y. *et al*. An electrochemical immunosensor for sensitive detection of Escherichia coli O157:H7 using C60 based biocompatible platform and enzyme functionalized Pt nanochains tracing tag. *Biosens. Bioelectron.* **49**, 485–491 (2013).
15. Lee, S. Y., Lee, J., Lee, H. S. & Chang, J. H. Rapid pathogen detection with bacterial-assembled magnetic mesoporous silica. *Biosens. Bioelectron.* **53**, 123–128 (2014).
16. Chen, L. M. *et al*. Heterogemini surfactant assisted synthesis of monodisperse icosahedral gold nanocrystals and their applications in electrochemical biosensing. *RSC Adv.* **6**, 31301–31307 (2016).
17. Zhang, L. *et al*. Hierarchical Flowerlike Gold Nanoparticles Labeled Immunochromatography Test Strip for Highly Sensitive Detection of Escherichia coli O157:H7. *Langmuir* **31**, 5537–5544 (2015).
18. Cui, X. *et al*. A remarkable sensitivity enhancement in a gold nanoparticle-based lateral flow immunoassay for the detection of Escherichia coli O157:H7. *RSC Adv.* **5**, 45092–45097 (2015).
19. Xue, H., Zhang, B., He, B., Wang, Z. & Chen, C. Rapid Immunochromatographic Assay for Escherichia coli O157:H7 in Bovine Milk Using IgY Labeled by Fe_3O_4/Au Composite Nanoparticles. *Food Sci. Technol. Res.* **22**, 53–58 (2016).
20. Song, C., Li, J., Liu, J. & Liu, Q. Simple sensitive rapid detection of Escherichia coli O157:H7 in food samples by label-free immunofluorescence strip sensor. *Talanta* **156–157**, 42–47 (2016).
21. Uusitalo, S. *et al*. Detection of Listeria innocua on roll-to-roll produced SERS substrates with gold nanoparticles. *RSC Adv.* **6**, 62981–62989 (2016).
22. Wu, C. & Xu, Q. H. Stable and functionable mesoporous silica-coated gold nanorods as sensitive localized surface plasmon resonance (LSPR) nanosensors. *Langmuir* **25**, 9441–9446 (2009).
23. Lee, Y. H., Chen, H. J., Xu, Q. H. & Wang, J. F. Refractive Index Sensitivities of Noble Metal Nanocrystals: The Effects of Multipolar Plasmon Resonances and the Metal Type. *J. Phys. Chem. C* **115**, 7997–8004 (2011).
24. Wang, C. & Irudayaraj, J. Gold nanorod probes for the detection of multiple pathogens. *Small* **4**, 2204–2208 (2008).
25. Li, C. *et al*. LSPR sensing of molecular biothiols based on noncoupled gold nanorods. *Langmuir* **26**, 9130–9135 (2010).
26. Zhang, Z. *et al*. Mesoporous Silica-Coated Gold Nanorods as a Light-Mediated Multifunctional Theranostic Platform for Cancer Treatment. *Adv. Mater.* **24**, 1418–1423 (2012).
27. Liu, J. *et al*. Gold nanorods coated with mesoporous silica shell as drug delivery system for remote near infrared light-activated release and potential phototherapy. *Small* **11**, 2323–2332 (2015).
28. Huang, X., Neretina, S. & El-Sayed, M. A. Gold nanorods: from synthesis and properties to biological and biomedical applications. *Adv. Mater.* **21**, 4880–4910 (2009).
29. Ming, T. *et al*. Strong polarization dependence of plasmon-enhanced fluorescence on single gold nanorods. *Nano Lett.* **9**, 3896–3903 (2009).
30. Ji, M. *et al*. Structurally Well-Defined Au@Cu2- x S Core-Shell Nanocrystals for Improved Cancer Treatment Based on Enhanced Photothermal Efficiency. *Adv. Mater.* **28**, 3094–3101 (2016).
31. Li, C. *et al*. Exploration of the growth process of ultrathin silica shells on the surface of gold nanorods by the localized surface plasmon resonance. *Nanotechnol.* **25**, 045704 (2014).

32. Yasukuni, R. *et al*. Silica-coated gold nanorod arrays for nanoplasmonics devices. *Langmuir* **29**, 12633–12637 (2013).
33. Abadeer, N. S., Fulop, G., Chen, S., Kall, M. & Murphy, C. J. Interactions of Bacterial Lipopolysaccharides with Gold Nanorod Surfaces Investigated by Refractometric Sensing. *ACS Appl. Mater. Interfaces* **7**, 24915–24925 (2015).
34. Peng, C. A. & Pachpinde, S. Longitudinal Plasmonic Detection of Glucose Using Gold Nanorods. *Nanomater. Nanotechnol.* **4**, 1 (2014).
35. Wang, J. *et al*. Hollow Au-Ag Nanoparticles Labeled Immunochromatography Strip for Highly Sensitive Detection of Clenbuterol. *Sci. Rep.* **7**, 41419 (2017).
36. Tian, L., Chen, E., Gandra, N., Abbas, A. & Singamaneni, S. Gold nanorods as plasmonic nanotransducers: distance-dependent refractive index sensitivity. *Langmuir* **28**, 17435–17442 (2012).
37. Hafner, H. La. J. H. Gold Nanorod Bioconjugates. *Chem. Mater.* **17**, 4636–4641 (2005).
38. Murphy, C. J. Oa. C. J. Quantitation of Metal Content in the Silver-Assisted Growth of Gold Nanorods. *J. Phys. Chem. B* **110**, 3990–3994 (2006).
39. Huang, Y., Ferhan, A. R. & Kim, D. H. Tunable scattered colors over a wide spectrum from a single nanoparticle. *Nanoscale* **5**, 7772–7775 (2013).
40. Wu, W. C. & Tracy, J. B. Large-Scale Silica Overcoating of Gold Nanorods with Tunable Shell Thicknesses. *Chem. Mater.* **27**, 2888–2894 (2015).
41. Tang, F., Li, L. & Chen, D. Mesoporous silica nanoparticles: synthesis, biocompatibility and drug delivery. *Adv. Mater.* **24**, 1504–1534 (2012).
42. Ouhenia-Ouadahi, K. *et al*. Photochromic-fluorescent-plasmonic nanomaterials: towards integrated three-component photoactive hybrid nanosystems. *Chem. Commun.* **50**, 7299–7302 (2014).
43. Su, H., Zhong, Y., Ming, T., Wang, J. & Wong, K. S. Extraordinary Surface Plasmon Coupled Emission Using Core/Shell Gold Nanorods. *J. Phys. Chem. C* **116**, 9259–9264 (2012).
44. Wu, W. C. & Tracy, J. B. Large-Scale Silica Overcoating of Gold Nanorods with Tunable Shell Thicknesses. *Chem. Mater.* **27**, 2888–2894 (2015).
45. Szunerits, S. & Boukherroub, R. Sensing using localised surface plasmon resonance sensors. *Chem. Commun.* **48**, 8999–9010 (2012).
46. DeSantis, C. J. & Skrabalak, S. E. Size-controlled synthesis of Au/Pd octopods with high refractive index sensitivity. *Langmuir* **28**, 9055–9062 (2012).
47. Jia, K. *et al*. Strong improvements of localized surface plasmon resonance sensitivity by using Au/Ag bimetallic nanostructures modified with polydopamine films. *ACS Appl. Mater. Interfaces* **6**, 219–227 (2014).
48. Shao, L., Ruan, Q., Jiang, R. & Wang, J. Macroscale colloidal noble metal nanocrystal arrays and their refractive index-based sensing characteristics. *Small* **10**, 802–811 (2014).
49. Bibikova, O. *et al*. Plasmon-Resonant Gold Nanostars With Variable Size as Contrast Agents for Imaging Applications. *IEEE J. Sel. Top. Quantum Electron.* **22**, 13–20 (2016).
50. Cao, J., Sun, T. & Grattan, K. T. V. Gold nanorod-based localized surface plasmon resonance biosensors: A review. *Sens. Actuators, B* **195**, 332–351 (2014).
51. Jung, L. S., Campbell, C. T., Chinowsky, T. M., Mar, M. N. & Yee, S. S. Quantitative Interpretation of the Response of Surface Plasmon Resonance Sensors to Adsorbed Films. *Langmuir* **14**, 5636–5648 (1998).
52. P, A. M. R. & Duyne, V. Single Silver Nanoparticles as Real-Time Optical Sensors with Zeptomole Sensitivity. *Nano Lett.* **3**, 1057–1062 (2003).
53. Zhu, J., Zhao, J.-wu & Li, J.-j. Location-Dependent Local Field Enhancement Along the Surface of the Metal–Dielectric Core–Shell Nanostructure. *Plasmonics* **5**, 311–318 (2010).
54. Huang, Y., Kannan, P., Zhang, L., Chen, T. & Kim, D.-H. Concave gold nanoparticle-based highly sensitive electrochemical IgG immunobiosensor for the detection of antibody–antigen interactions. *RSC Adv.* **5**, 58478–58484 (2015).
55. Gorelikov, I. & Matsuura, N. Single-step coating of mesoporous silica on cetyltrimethyl ammonium bromide-capped nanoparticles. *Nano Lett.* **8**, 369–373 (2008).

Acknowledgements

We thank the Natural Science Foundation of Hubei (Program No. 2011CDC068), the State Key Laboratory of Agricultural Microbiology (Program No. AMLKF201205), the Fundamental Research Funds for the Central Universities (Program No. 2662015PY153), the Natural Science Foundation of China (21404110, 51473179, 51303195, 21304105), Ningbo Science and Technology Bureau (Grant 2014B82010 and 2015C110031), Youth Innovation Promotion Association of Chinese Academy of Sciences (2016268, 2017337).

Author Contributions

L-P. S., Y-J. H. and Z-D. X. designed the research; L-P. S. and L. Z. performed the experiments; L-P. S., L. Z., L-M. C. and G-G. Z. analyzed the data; Y-J. H., Z-Y. S., J-W. Z., Z-D. X. and T. C. contributed to the reagents/materials/analysis tools; L-P. S., L. Z. and Y-J. H. wrote the paper; All authors approved the final manuscript.

Additional Information

Supplementary information accompanies this paper at doi:10.1038/s41598-017-03495-1

Competing Interests: The authors declare that they have no competing interests.

Publisher's note: Springer Nature remains neutral with regard to jurisdictional claims in published maps and institutional affiliations.